




Original Research

Aldo-keto Reductase 1B10 (AKR1B10) Suppresses Sensitivity of Ferroptosis in TNBC by Activating the AKT/GSK3 β /Nrf2/GPX4 Axis

Shanli Wu^{1,2,†} , Gun Yang^{3,†}, Xiaosha Wen⁴, Yi Lin⁴, Shenglong Wang⁵, Jing Wang⁴, Quan Liu^{6,*} , Dixian Luo^{1,6,*} 

¹The First School of Clinical Medicine, Southern Medical University, 510000 Guangzhou, Guangdong, China

²Blood Transfusion Department, Shenzhen Nanshan People's Hospital, 518052 Shenzhen, Guangdong, China

³Institute of Pharmacy and Pharmacology, School of Pharmaceutical Science, Hengyang Medical School, University of South China, 421001 Hengyang, Hunan, China

⁴Laboratory Medicine Centre, Shenzhen Nanshan People's Hospital, 518052 Shenzhen, Guangdong, China

⁵First Clinical Medical College of Ningxia Medical University, 750000 Yinchuan, Ningxia, China

⁶Medical Laboratory Center, the Third Affiliated Hospital (The Affiliated Luohu Hospital) of Shenzhen University, 518001, Shenzhen, Guangdong, China

*Correspondence: liu_quan2020@163.com (Quan Liu); luodixian_2@163.com (Dixian Luo)

†These authors contributed equally.

Academic Editor: Jordi Sastre-Serra

Submitted: 27 December 2024 Revised: 1 May 2025 Accepted: 26 May 2025 Published: 27 June 2025

Abstract

Background: Aldo-keto reductase 1B10 (AKR1B10) is expressed in various malignant tissues. Several studies have highlighted the essential function of AKR1B10 in lipid metabolism and in the detoxification of lipid peroxides. The aim of this research was to explore the role of AKR1B10 in the susceptibility of MDA-MB-231 cells to ferroptosis. These cells serve as a model for triple-negative breast cancer (TNBC). **Methods:** Lentiviral transfection was used to establish stable cell lines with high or low expression of AKR1B10. Our model of ferroptosis used the ferroptosis activator RSL3, and the specific ferroptosis inhibitor ferrostatin-1 (Fer-1) to rescue cell death. Stable cell lines were treated with the specific inhibitor OSU-T315 directed against phosphorylation of Ser473 in protein kinase B (AKT) and Ser9 in glycogen synthase kinase 3 beta (GSK3 β), either alone or in combination with RSL3. A fatty acid stress model was established using palmitic acid (PA) or arachidonic acid (AA), either in the presence or absence of serum starvation and with or without co-treatment with RSL3. Cell viability was evaluated with the cell counting kit-8 (CCK8) assay and lipid peroxidation levels by flow cytometry after staining with C11 BODIPY 581/591. Exploration of the underlying mechanisms was conducted through RNA sequencing and bioinformatics analysis. Western blotting was performed to evaluate protein levels, and quantitative real-time polymerase chain reaction (qPCR) was used to evaluate transcript levels. **Results:** Western blot and qPCR analyses validated the successful establishment of stable MDA-MB-231 cell lines with and without AKR1B10 overexpression. Cell viability and lipid reactive oxygen species (ROS) assays showed that AKR1B10 suppressed ferroptosis in the RSL3-induced cell death model. Kyoto Encyclopedia of Genes and Genomes (KEGG) and Gene Set Enrichment Analysis (GSEA) analyses indicated the phosphatidylinositol 3-kinase (PI3K)-AKT pathway was likely to play a role in the underlying mechanisms. AKR1B10 increased the expression of glutathione peroxidase 4 (GPX4), thus potentially implicating the AKT/GSK3 β /nuclear factor erythroid 2-related factor 2 (NRF2)/GPX4 pathway in the mechanism. These changes in protein levels were also observed by Western blot analysis after 6 h of RSL3 treatment. Under the influence of RSL3, the transcript levels of NRF2-related genes including *GPX4*, ferritin heavy chain 1 (*FTH1*), heme oxygenase 1 (*HO-1*), and NAD(P)H quinone dehydrogenase 1 (*NQO-1*) were significantly elevated in the AKR1B10 overexpression cell line, whereas that of prostaglandin-endoperoxide synthase 2 (*PTGS2*) was significantly reduced. Similar changes were observed after treatment with OSU-T315. AKR1B10 was found to suppress the sensitivity to ferroptosis induced by treatment with OSU-T315, PA, or AA. These phenomena were rescued by the ferroptosis inhibitor Fer-1. **Conclusions:** AKR1B10 appears to be an important mechanism protecting MDA-MB-231 cells from ferroptosis, possibly through the AKT Ser473/GSK3 β Ser9/NRF2/GPX4 pathway. AKR1B10 may be a key factor underlying the therapeutic effect of RSL3 under different exogenous fatty acid microenvironments.

Keywords: aldo-keto reductase family 1 member B10; ferroptosis; triple-negative breast neoplasms; NFE2L2

1. Introduction

Ferroptosis is a regulated form of cell death characterized by iron dependence and in which the driving mechanism is lipid peroxidation [1–3]. It is intricately associated with various biological processes, including development, aging, immune response, and cancer. Numerous metabolic pathways contribute directly or indirectly to the regulation of ferroptosis by balancing iron accumulation or lipid per-

oxidation with the metabolic processing of iron, lipids, and amino acids, along with certain degradation processes such as the ubiquitin-proteasome system (UPS) and macroautophagy/autophagy [4]. RSL3 is a known inducer of ferroptosis and selectively exerts a lethal effect on cells harboring oncogenic rat sarcoma (*RAS*) mutations. This compound targets the selenium-rich enzyme Glutathione Peroxidase 4 (GPX4) [5], which is an inhibitor of ferroptosis. The ac-



tivity of GPX4 relies on glutathione (GSH) to facilitate the conversion of phospholipid hydroperoxide (PLOOH) into a harmless form [6], thereby effectively shielding cells from lipid peroxidation-induced damage.

Glycerophospholipids are crucial components of the lipid bilayer and significantly influence the occurrence of ferroptosis through the formation of oxidized phosphatidylcholine (OxPC). Among these, 1-palmitoyl-2-(5'-oxo-valeroyl)-sn-glycero-3-phosphocholine (POVPC) and 1-palmitoyl-2-(9'-oxo-nonoyl)-sn-glycero-3-phosphocholine (PONPC) cause significant cardiac toxicity depending on their concentration and exposure time. The accumulation of POVPC and PONPC markedly decreases the cellular activity of GPX4 in cells, rendering them more vulnerable to ferroptosis [7]. Aldo-keto reductase 1B10 (AKR1B10) has a detoxification function for lipid peroxides. Members of the AKR1B family effectively reduce substances such as the phospholipid aldehyde POVPC [8]. Consequently, AKR1B10 may be vital for maintaining the integrity of cell membranes and protecting cells from oxidative stress-induced damage.

AKR1B10 is absent in normal breast tissue, but expressed at significant levels in some primary and metastatic breast cancer samples, with elevated expression being strongly linked to poor prognosis [9]. In a case-control study, our research team found that the serum AKR1B10 level was markedly higher in individuals with localized or metastatic breast cancer, and was positively correlated with the expression of AKR1B10 in cancerous tissues. Furthermore, the serum AKR1B10 level fell significantly within three days after the excision of the primary tumor [10], thus reinforcing the connection between its expression and disease status in breast cancer. The triple-negative breast cancer (TNBC) phenotype has a poor prognosis and a high tendency for metastasis. The occurrence, growth, and metastasis of this aggressive breast cancer subtype are known to be affected by dysregulated lipid metabolism. In the present study, we utilized RSL3 as an inducer of ferroptosis and introduced different exogenous fatty acids to simulate various lipid microenvironments. This allowed us to explore the mechanism by which ectopic AKR1B10 expression can affect the survival of TNBC cells.

2. Materials and Methods

2.1 Cell Culture

The cells used in this study were the human embryonic kidney cell line HEK293T (CL-0005, Procell, Wuhan, Hubei, China) and the human triple-negative breast cancer cell line MDA-MB-231 (CL-0150, Procell, Wuhan, Hubei, China). Both were maintained in DMEM medium (11995065, Gibco, Shanghai, China) enriched with 10% fetal bovine serum (FBS, 164210, Procell, Wuhan, Hubei, China) and containing 100 U/mL penicillin and 100 U/mL streptomycin. Penicillin/streptomycin was obtained from NCM (C100C5, NCM, Suzhou, Jiangsu, China). Cells

were grown at 37 °C in an atmosphere containing 5% carbon dioxide. The cell lines used in this study underwent short tandem repeat (STR) profiling and tested negative for mycoplasma contamination.

Lentiviral technology was used to construct MDA-MB-231 cell lines that were stably transfected with vector and AKR1B10 and then screened with puromycin. The cell model for induction of ferroptosis was established using RSL3 (HY-100218A, MCE, Shanghai, China). Initial verification of the ferroptosis cell model was conducted using a 96-well plate format. MDA-MB-231 cells with high or low expression of AKR1B10 were exposed to varying concentrations (0–10 µM) of RSL3, either alone or in combination with the specific inhibitor OSU-T315 (0–5 µM), for 24 h. For the experiments involving fatty acid pretreatment, cells were first incubated for 2 h with fatty acids [300 µM palmitic acid (PA) or 50 µM arachidonic acid (AA)] dissolved in basal or complete culture medium, then treated with RSL3 (0–10 µM) for 24 h. Cell viability was assessed using a cell counting kit-8 (CCK8) assay following the manufacturer's protocol. For the experimental protocol, vector and AKR1B10 cells were divided into the following treatment groups: RSL3 at various concentrations (0–10 µM) for 24 h, OSU-T315 (T5485, Topscience, Shanghai, China) at various concentrations (0–5 µM) for 24 h, a combination of OSU-T315 (2.5 µM or 5 µM) and RSL3 (2.5 µM) for 24 h, a combination of PA (300 µM, KC001, Xi'an Kunchuang, Xi'an, Shaanxi, China) and RSL3 (0–10 µM) for 24 h, a combination of AA (50 µM, KC014, Xi'an Kunchuang, Xi'an, Shaanxi, China) and RSL3 (0–10 µM) for 24 h, and fatty acids at various concentrations (0–600 µM PA or 0–100 µM AA) for 24 h or 48 h. For cell rescue experiments, the ferroptosis inhibitor ferrostatin-1 (Fer-1, 5 µM, S7243, Selleck, Shanghai, China) was applied 2 h prior to single or combination therapies and maintained throughout treatment.

2.2 Plasmids and Lentiviral Transfection

The AKR1B10 DNA sequence was retrieved from the NCBI website (<https://www.ncbi.nlm.nih.gov>). The detailed sequence can be found in the **Supplementary Materials**. Lentiviral transduction was performed using the pCDH plasmid to establish MDA-MB-231 cell lines with or without AKR1B10 overexpression. Plasmids were obtained from Shanghai Kelei Biotechnology (Shanghai, China) and transfected using Lipofectamine 2000 reagent (11668019, Invitrogen, Shanghai, China). A mixture (4:3:1) of the target plasmid, packaging plasmid (psPAX2), and envelope plasmid (pMD2.G) was introduced into HEK293T cells to generate lentivirus and subsequently harvested to infect MDA-MB-231 cells. After 48 h of infection, 2 µg/mL puromycin (ST551, Beyotime, Shanghai, China) was added to select for stably expressing cell lines.

2.3 Cell Viability Assay

A total of 3000 cells were seeded (100 μ L per well) in a 96-well plate and incubated overnight at 37 °C. Complete or basic culture medium containing various concentrations of drugs was added and the cells incubated for the required time. The medium was subsequently substituted with complete medium containing 10% CCK8 reagent (C6005, NCM, Suzhou, Jiangsu, China), and the absorbance was recorded at 450 nm using a microplate reader (Spectra-Max® iD3, Molecular Devices, Shanghai, China). Cell viability was calculated using the following formula: cell viability (%) = $(A_{\text{sample}} - A_{\text{blank}})/(A_{\text{control}} - A_{\text{blank}}) \times 100$, where A represents the absorbance value.

2.4 RNA Sequencing

MDA-MB-231 cells were cultured in 6-well plates, and stable cell lines of vector and AKR1B10 were established via lentiviral infection. Total RNA was extracted and purified from these cells using TRIzol reagent (15596018, Thermo Fisher Scientific, Shanghai, China) as recommended by the manufacturer. Oligo (dT) magnetic beads (61005, Thermo Fisher Scientific, Shanghai, China) were used to specifically isolate polyA mRNA from the samples. mRNA fragmentation occurred at elevated temperatures using a magnesium ion disruption kit (E6150S, NEB, Beijing, China), followed by cDNA synthesis using a reverse transcriptase kit (1896649, Thermo Fisher Scientific, Shanghai, China). The cDNA was subsequently converted into dsDNA through a double-stranding reaction using *E. coli* DNA polymerase I (m0209, NEB, Beijing, China) and RNase H (m0297, NEB, Beijing, China), during which dUTP solution (R0133, Thermo Fisher Scientific, Shanghai, China) was incorporated. End repair was then performed, and the product was subsequently purified using magnetic bead technology. A cDNA library was constructed via PCR amplification, and paired-end sequencing was carried out on the Illumina Novaseq™ 6000 platform (LC Bio Technology Co., Ltd., Hangzhou, China) using standard operating procedures.

Data analysis and visualization were performed using the online platform <https://www.omicstudio.cn/home>. For the analysis of differentially expressed genes (DEGs) and associated Kyoto Encyclopedia of Genes and Genomes (KEGG) pathways, datasets were screened using predefined thresholds. Gene expression levels were compared between the AKR1B10 expression group and the control vector group using the following specific screening criteria: Fold-Change (FC) ≥ 1.25 , Fragments Per Kilobase of transcript per Million mapped reads (FPKM) > 1 , and *p*-value < 0.05 . In contrast, Gene Set Enrichment Analysis (GSEA) was performed without any preliminary data filtering. KEGG pathway analysis was performed to identify the biological pathways most relevant to the study. GSEA does not rely on predefined threshold values for differential gene selection and was conducted to identify significantly

enriched biological pathways. Gene sets for GSEA were obtained from public databases such as the Molecular Signatures Database (MSigDB).

2.5 Measurement of Lipid Peroxidation

After discarding the culture medium, cells were incubated with complete medium containing 10 μ M C11 581/591 BODIPY (D3861, Invitrogen, Shanghai, China) for 1 h, then rinsed with PBS (G4202, Servicebio, Wuhan, Hubei, China), digested with trypsin, and resuspended in 500 μ L of PBS. To quantify lipid reactive oxygen species (ROS) levels, fluorescence intensity values in the FITC channel were assessed using flow cytometry (NAVIOS, Beckman Coulter, Brea, CA, USA). FlowJo v10.8.1 software (FlowJo LLC, Ashland, OR, USA) was employed for data analysis. The fluorescence intensity of the control group was used to set the gating threshold, ensuring that signals from negative cells were confined to the designated negative region. The fluorescence intensities of all groups were then compared to determine the proportion of positive cells. Data from replicate wells (FITC measurements) were combined and presented as the mean \pm SD.

2.6 Western Blotting

Following cell lysis, the total protein content was isolated using RIPA buffer (P0013B, Beyotime, Shanghai, China) containing protease inhibitor (G2008, Servicebio, Wuhan, Hubei, China) and phosphatase inhibitor (G2007, Servicebio, Wuhan, Hubei, China) to preserve protein integrity. The extracted proteins were then resolved via sodium dodecyl sulfate polyacrylamide gel electrophoresis (SDS-PAGE) (P0014C, Beyotime, Shanghai, China) and transferred onto a PVDF membrane (ISEQ00010, Merck, Tipperary, Ireland) using transfer buffer (E173-01, Genstar, Beijing, China). The membrane was then blocked with a 5% non-fat milk solution (232100, BD Difco, Franklin Lakes, NJ, USA) for 2 h to prevent nonspecific binding. Following this, the membrane was incubated overnight at 4 °C with the primary antibody and then washed three times for 10 minutes each before incubation with the secondary antibody. The primary antibodies used in this study were as follows: AKR1B10 (1:1000, 18252-1-AP, Proteintech, Wuhan, Hubei, China), protein kinase B (AKT, 1:5000, ab179463, Abcam, Shanghai, China), Phospho-AKT Ser473 (1:2000, 4060T, CST, Danvers, MA, USA), glycogen synthase kinase 3 beta (GSK-3 β , 1:1000, 12456T, CST, Danvers, MA, USA), Phospho-GSK-3 β Ser9 (1:1000, 5558T, CST, Danvers, MA, USA), erythroid 2-related factor 2 (NRF2, 1:500, 12721T, CST, Danvers, MA, USA), Kelch-like ECH-associated protein 1 (KEAP1, 1:1000, D6B12, CST, Danvers, MA, USA), and GPX4 (1:1000, 52455T, CST, Danvers, MA, USA). The secondary antibody was goat anti-rabbit IgG conjugated to horseradish peroxidase (1:10,000, 7074, CST, Danvers, MA, USA). The PVDF membrane was immersed in the secondary an-

tibody solution and incubated at room temperature for 1 h. After three membrane washes, the protein bands were detected using an ECL substrate (BL520B, Biosharp, Tallinn, Estonia), and the protein levels were evaluated using a chemiluminescence imaging system (OI 600 MF, BIO-OI, Guangzhou, China). ImageJ 1.53t software (National Institutes of Health, Bethesda, MD, USA) was used to quantify the signal intensity.

The relative expression level of the target protein was calculated using the following formula: relative expression of target protein = (signal intensity of target protein)/(signal intensity of internal reference protein). The relative expression level of the target protein in the experimental groups was determined by normalizing to the control group, which is defined as 1.

2.7 Quantitative Real-Time Polymerase Chain Reaction (qPCR)

RNA was extracted from adherent cells using the TransZol Regular RNA Extraction Kit (ET101-01-V2, TransGen, Beijing, China) as recommended by the manufacturer. Briefly, cells were lysed with guanidine isothiocyanate (G108673, Aladdin, Shanghai, China) before adding the RNA extraction reagent. The solution was then separated into a colorless aqueous phase and a pink organic phase. RNA was present in the aqueous phase and was precipitated and recovered using isopropanol. qPCR experiments were conducted using HiScript III RT SuperMix (R323, Vazyme, Nanjing, Jiangsu, China) and PerfectStart® Green qPCR SuperMix (AQ602, TransGen, Beijing, China). The extracted RNA was reverse transcribed into cDNA and then amplified with the following human-specific primers (Shenzhen Hechengyuan Biotechnology Co., Ltd.): *AKR1B10*, 5'-CAGCAACAGAGAGCAGGACG-3' and 5'-TGCCAAGAGGAGACTTCCAA-3'; *GPX4*, 5'-AAGATCCAACCAAGGGCAA-3', and 5'-AGACGGTGTC CAACTTGGTG-3'; heme oxygenase 1 (*HO-1*), 5'-AC TGCGTTCCTGCTCAACAT-3' and 5'-GGGGGCAGA ATCTTGCACT-3'; NAD(P)H quinone dehydrogenase 1 (*NQO-1*), 5'-GCTGGTTTGAGCGAGTGTTT-3' and 5'-C TGCCTTCTTACTCCGGAAGG-3'; ferritin heavy chain 1 (*FTH1*), 5'-ACTACCACAGGACTCAGAGG-3' and 5'-CAGTCATCACAGTCTGGTTTCTTG-3'; prostaglandin-endoperoxide synthase 2 (*PTGS2*), 5'-GCAAATTGCTGG CAGGGTTG-3' and 5'-GCTCTGGTCAATGGAAGCCT -3'. The Applied Biosystems 7300 Real-Time PCR System (Thermo Fisher Scientific, Foster City, CA, USA) was used to analyze gene expression.

The Ct value of the target gene was first normalized to the Ct value of an internal reference gene (ΔCt). Subsequently, the difference in ΔCt between the target sample and the control sample was calculated ($\Delta\Delta Ct$), followed by the calculation of the relative expression level of the target gene using the formula $2^{-\Delta\Delta Ct}$.

2.8 Statistical Analysis

Each experimental procedure was carried out in triplicate. Statistical analysis was conducted using GraphPad Prism 10.3.0 software (GraphPad Software Inc., La Jolla, CA, USA). Data are presented as the mean \pm SD. Comparisons between two groups were conducted using a two-tailed Student's *t*-test. Comparisons among multiple groups were performed using either one-way ANOVA or two-way ANOVA, followed by post hoc multiple comparison analyses using Tukey's, Dunnett's, and Sidak's tests. A *p*-value < 0.05 was considered statistically significant. For complex multiple comparison analysis, the Compact Letter Display (CLD) was used to replace the commonly used asterisks or *p*-values to present pairwise comparison results. Each experimental group was designated with at least one letter, with shared letters between groups indicating statistically insignificant differences ($p \geq 0.05$).

3. Results

3.1 Overexpression of *AKR1B10* Protects MDA-MB-231 Cells From Ferroptosis

Lentiviral technology was used to construct stable cell lines with either *AKR1B10* overexpression or the control vector. Ectopic expression of *AKR1B10* was confirmed at both the protein and mRNA levels (Fig. 1A,B). To explore how *AKR1B10* influences the therapeutic efficacy of RSL3, we performed an *in vitro* assessment of the effect of the drug treatment. Overexpression of *AKR1B10* caused a marked shift in the cell survival curve, indicating a potential protective effect (Fig. 1C). Furthermore, the ferroptosis inhibitor Fer-1 mitigated the cell death induced by RSL3 (Fig. 1D). Additionally, the C11 BODIPY 581/591 probe was used to label cells in order to assess the level of lipid peroxidation by flow cytometry. *AKR1B10* overexpression was associated with a significant decrease ($p < 0.01$) in lipid peroxidation within the cells (Fig. 1E,F), suggesting a potential protective function for *AKR1B10* against ferroptosis in MDA-MB-231 cells.

3.2 RNA Sequencing Suggests that the Protective Role of *AKR1B10* in Ferroptosis May Be Linked to the Phosphatidylinositol 3-Kinase/Protein Kinase B (PI3K-AKT) Signaling Pathway

We next conducted RNA-seq analysis to study the mechanism underlying the effect of RSL3 treatment in the presence of *AKR1B10* overexpression. This identified a set of DEGs (Fig. 2A), as shown in the heat map in Fig. 2B. KEGG pathway analysis of these DEGs showed significant enrichment of the top 20 pathways across various biological processes, including metabolism, PI3K-AKT, RAS and other signaling pathways (Fig. 2C). Further statistical evaluation of the classical pathways indicated significant enrichment in the PI3K-AKT pathway (Fig. 2D). To investigate the potential molecular mechanisms in more detail, GSEA was performed on the complete RNA-seq gene set, as well as KEGG pathway analysis. The results re-

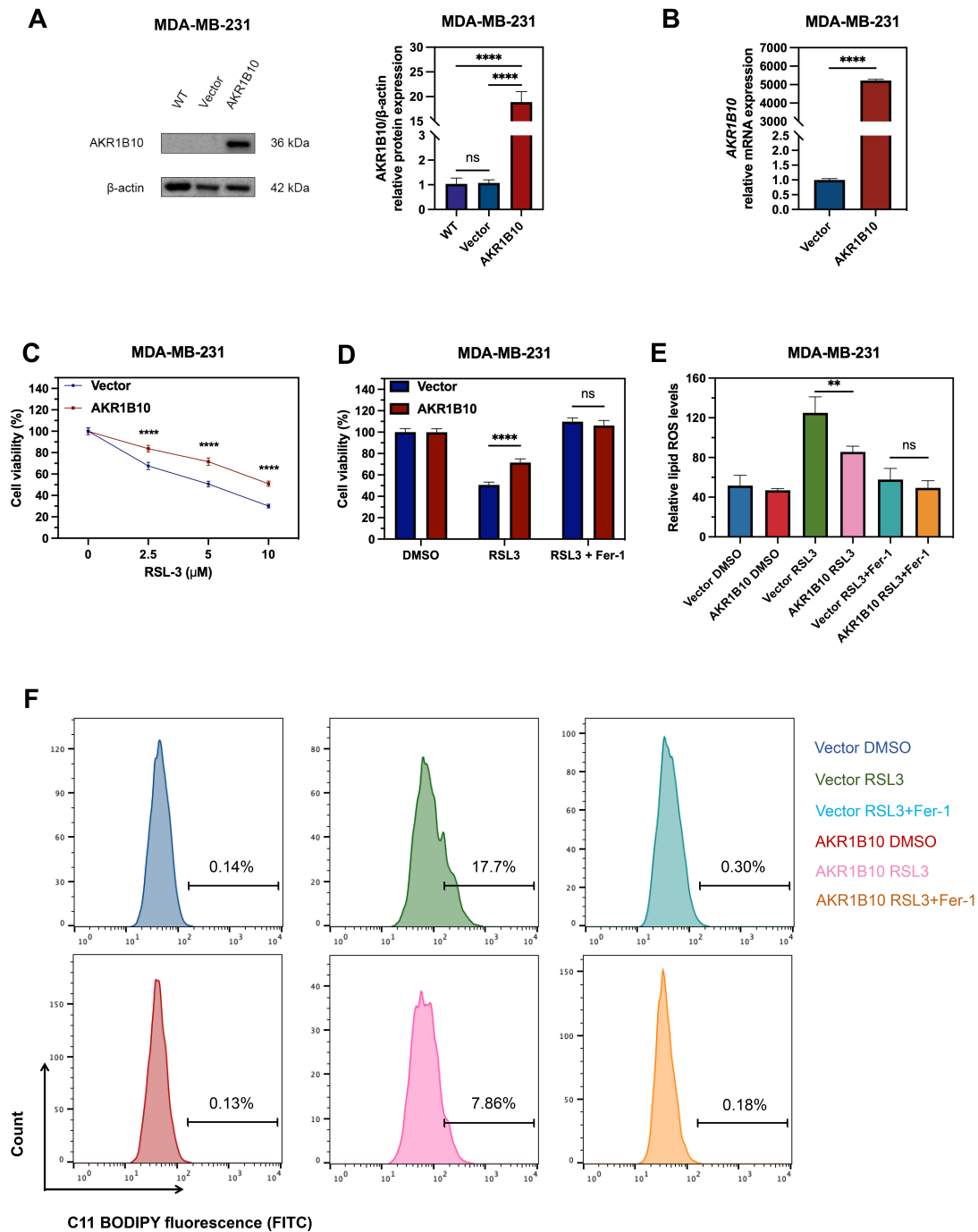


Fig. 1. Overexpression of aldo-keto reductase 1B10 (AKR1B10) protects MDA-MB-231 cells from ferroptosis. (A) Ectopic expression of the AKR1B10 protein in triple-negative breast cancer MDA-MB-231 cells was confirmed by Western blot analysis ($n = 3$). (B) Quantitative real-time polymerase chain reaction (qPCR) was used to verify the establishment of the control vector and AKR1B10 stably transfected cell lines ($n = 4$). (C) Cell viability was evaluated using the cell counting kit-8 (CCK8) assay following treatment with varying concentrations of the ferroptosis activator RSL3 ($n = 6$). (D) Cells were pretreated with the ferroptosis-specific inhibitor ferrostatin-1 (Fer-1) ($5 \mu\text{M}$) before co-incubation with RSL3 ($5 \mu\text{M}$) for 24 h. Cell viability was then assessed with the CCK8 assay ($n = 6$). (E,F) Following the same treatment as in (D) for 8 h, cells were labeled with the C11 BODIPY581/591 probe to measure lipid peroxidation levels using flow cytometry ($n = 3$). The overall levels of lipid reactive oxygen species (ROS) were presented as the mean \pm SD of the fluorescence intensity of lipid peroxidation (FITC) (E). After setting a negative gate based on the control cells, the percentage of positive lipid ROS in each group was shown in (F). The data were analyzed by two-tailed Student's t -test (B), one-way ANOVA corrected by Tukey's (A,E) test, and two-way ANOVA corrected by Sidak's (C,D) test. ns, not significant; ** $p < 0.01$, **** $p < 0.0001$.

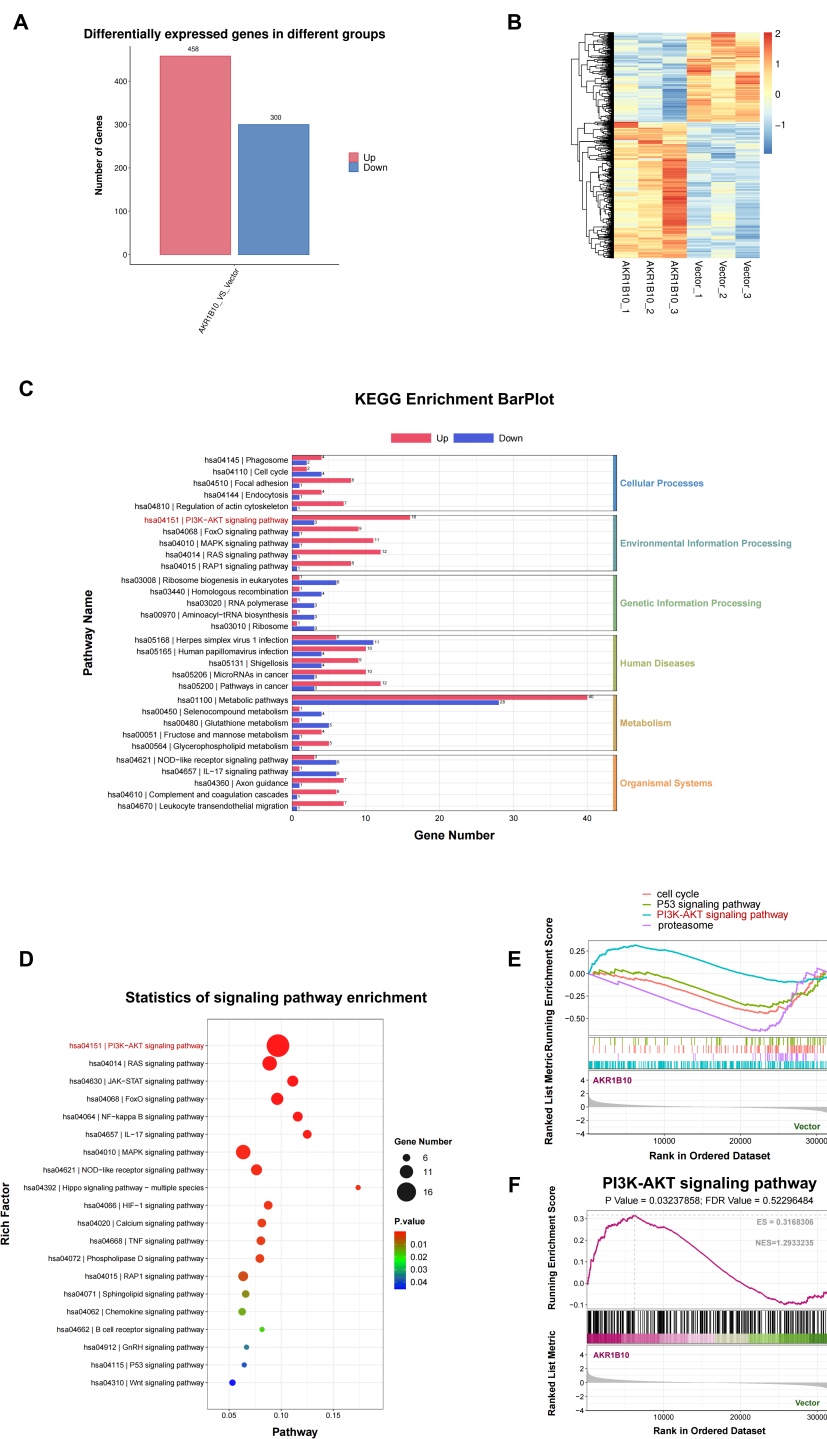


Fig. 2. RNA sequencing revealed that the protective role of AKR1B10 in ferroptosis may be related to the phosphatidylinositol 3-kinase/protein kinase B (PI3K-AKT) signaling pathway. Gene expression changes caused by AKR1B10 overexpression were detected by RNA-seq technology. The results are presented as differentially expressed genes (DEGs) (A) and as a heatmap (B). (C) The DEGs identified in (A) underwent Kyoto Encyclopedia of Genes and Genomes (KEGG) pathway analysis, with the top 20 pathways showing significant enrichment. (D) Statistical analysis of the relative signaling pathways revealed that the PI3K-AKT pathway was the most significantly enriched. (E,F) KEGG pathway analysis using Gene Set Enrichment Analysis (GSEA) revealed significant differences in ferroptosis-related pathways, including PI3K-AKT, p53, the proteasome, and the cell cycle. This figure was generated using the online platform <https://www.omicstudio.cn/home>.

vealed notable differences in ferroptosis-related pathways, including PI3K-AKT, p53, proteasome, and the cell cycle (Fig. 2E,F).

3.3 AKR1B10 Mediates Decreased Sensitivity to Ferroptosis via the AKT/GSK3 β /NRF2/GPX4 Axis

GPX4 facilitates the reduction in lipid peroxides within the complex environment of the cellular membrane. Under normal conditions, we observed that AKR1B10 overexpression resulted in elevated GPX4 ($p < 0.001$) protein levels (Fig. 3A). To further elucidate the mechanism by which AKR1B10 modulates GPX4, we assessed the phosphorylation status of AKT protein, as suggested by involvement of the PI3K-AKT pathway in the previous RNA sequencing enrichment. AKR1B10 overexpression was found to increase the ratio of p-AKT Ser473/AKT ($p < 0.001$) and p-GSK3 β Ser9/GSK3 β ($p < 0.01$). The level of NRF2 protein was also elevated ($p < 0.05$) (Fig. 3B). NRF2 is a key upstream regulator of GPX4 and is tightly controlled by regulatory factors such as GSK3 β and KEAP1. These factors influence the nuclear import of NRF2, as well as its binding to antioxidant response elements (ARE), nuclear export, and degradation in both normal and stressful environments. KEAP1 facilitates the ubiquitination and degradation of NRF2 and also serves as a crucial sensor for oxidative and electrical stress [11]. Phosphorylated AKT (Ser473) inhibits the activity of GSK3 β by phosphorylating its Ser9 residue. In the resting state, GSK3 β is unphosphorylated and active and continuously phosphorylates downstream components resulting in the constitutive degradation of NRF2. The present study found that AKR1B10 increases the phosphorylation of AKT at Ser473, thereby causing it to phosphorylate and hence inactivate GSK3 β (Fig. 3B). Inactivation of GSK3 β overcomes the suppression of NRF2 entry into the nucleus [12], thus ultimately stabilizing NRF2 expression. Western blot analysis revealed differential expression of associated proteins following treatment with varying concentrations of RSL3 for 6 h (Fig. 3C). As the drug concentration increased, RSL3 treatment triggered an oxidative stress response in cells, characterized by increased phosphorylation of AKT at Ser473 and GSK3 β at Ser9. This cascade leads to increased protein levels of NRF2 and its downstream target GPX4, especially in AKR1B10-overexpressing cells. During the induction of ferroptosis mediated by RSL3, elevated AKR1B10 expression promotes higher phosphorylation of AKT and GSK3, while also increasing activation of the NRF2 system. Notably, AKR1B10 itself was previously shown to be directly transcribed by NRF2 [13]. The current study highlights this positive feedback loop which strengthens the antioxidant defense mechanisms of tumor cells.

To further investigate the role of the AKT Ser473/GSK3 β Ser9 pathway in ferroptosis, MDA-MB-231 cells were treated with the specific inhibitor OSU-T315. This novel inhibitor exerts its therapeutic effect by promoting the dephosphorylation of AKT at

Ser473 and of GSK3 β at Ser9. Lee *et al.* [14] previously reported that OSU-315 induces autophagy and apoptosis in MDA-MB-231 cells. MDA-MB-231 vector and MDA-MB-231 AKR1B10 cells were treated with varying concentrations of OSU-T315. In the 0–5 μ M concentration range of OSU-T315, AKR1B10 had no significant effect on cell viability (Fig. 3E). However, the combination of RSL3 and OSU-T315 (Fig. 3F) resulted in a reduction in cell survival compared to RSL3 treatment alone (Fig. 3D). This combined effect could still be rescued by the specific ferroptosis inhibitor Fer-1 (Fig. 3F), suggesting that OSU-T315 can enhance the cell sensitivity to ferroptosis induced by RSL3. We next examined mRNA expression to assess whether this process involves the differential expression of NRF2-dependent antioxidant genes. The results of qPCR showed that RSL3 induced AKR1B10 high-expression cells to increase the transcription levels of *GPX4* ($p < 0.01$), *FTH1*, $p < 0.0001$, *HO-1*, $p < 0.001$, and *NQO-1*, $p < 0.0001$, while decreasing that of *PTGS2*, $p < 0.0001$ (Fig. 3G), thereby protecting cells from ferroptosis. Similar effects were observed in cells treated with OSU-T315 (Fig. 3H). We speculated these changes may be due to downstream NRF2-related detoxifying proteins that inhibit phosphorylation of AKT Ser473 and GSK3 β Ser9, thereby reducing the sensitivity of AKR1B10 overexpressing cells to ferroptosis.

3.4 AKR1B10 May Be a Key Factor in the Efficacy of RSL3 Therapy in the Presence of Different Exogenous Fatty Acids

Given the pivotal role of AKR1B10 in fatty acid metabolism, we next investigated the impact of various fatty acid environments on the therapeutic efficacy of ferroptosis in tumor cells. Previous research found that mice injected with MDA-MB-231-Luc cells with high AKR1B10 expression showed a marked increase in lung tumor burden [15]. High-fat diets are known to exacerbate cancer progression. Palmitic acid (PA), a saturated fatty acid, was previously identified as a promoter of cancer metastasis [16], while arachidonic acid (AA) is a common polyunsaturated fatty acid (PUFA), that was recently studied in relation to ferroptosis. Our earlier work showed that AKR1B10 reduces the sensitivity of MDA-MB-231 cells to RSL3-induced ferroptosis. To explore the potential of combined fatty acid and RSL3 therapy, cells were pretreated with 300 μ M PA or 50 μ M AA for 2 h in either complete or serum-free medium. These conditions simulate the complex fatty acid environment that tumor cells encounter during lung metastasis and in other biological contexts. The cells were then treated with RSL3 for 24 h to simulate lipid peroxide-induced stress damage. The combination of these fatty acids with RSL3 resulted in greater cytotoxicity than single-agent treatments, regardless of the presence of serum during pretreatment. Moreover, the sensitizing effect of these therapies could be rescued by Fer-1. AKR1B10 remained the determining factor for differential cell viability

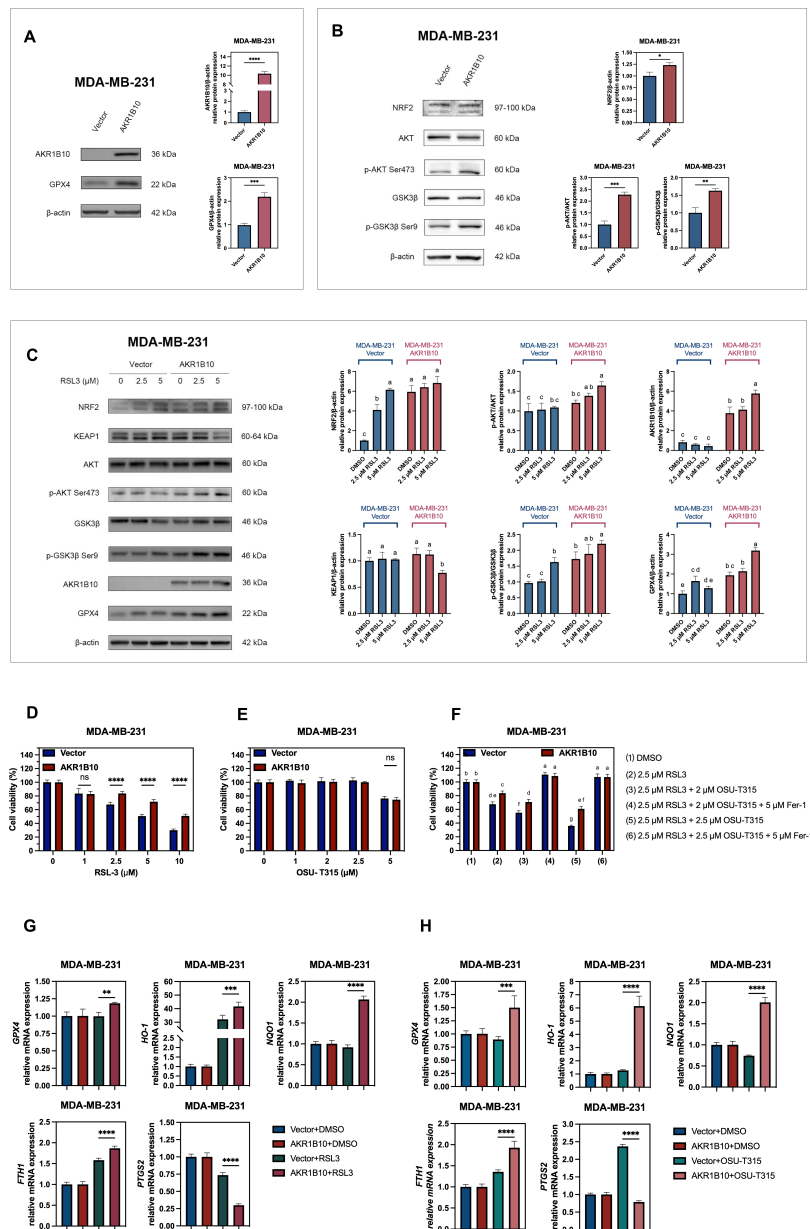


Fig. 3. AKR1B10 reduces sensitivity to ferroptosis via the AKT Ser473/Glycogen Synthase Kinase 3 Beta (GSK3 β) Ser9/Nuclear factor erythroid 2-related factor 2 (NRF2)/glutathione peroxidase 4 (GPX4) axis. (A) Western blot analysis of GPX4 protein levels in cells with ectopic expression of AKR1B10. (B) Western blot analysis showing the ratio of p-AKT/AKT and p-GSK3 β /GSK3 β , as well as the level of NRF2 protein in MDA-MB-231 cells with or without AKR1B10 overexpression. (C) Western blot showing the expression levels of related proteins following treatment of MDA-MB-231 cells (with or without AKR1B10 overexpression) with different concentrations of the ferroptosis activator RSL3 for 6 h. (D) CCK8 assay results showing cell viability after treatment of MDA-MB-231 cells (with or without AKR1B10 overexpression) with different concentrations of RSL3 for 24 h (n = 6). (E) CCK8 assay results showing cell viability after treatment of MDA-MB-231 cells (with or without AKR1B10 overexpression) with different concentrations of OSU-T315 for 24 h (n = 6). (F) CCK8 assay results showing cell viability after treatment of MDA-MB-231 cells (with or without AKR1B10 overexpression) with 2.5 μ M RSL3, along with various combinations of OSU-T315 for 24 h. The ferroptosis inhibitor Fer-1 was used to rescue from cell death (n = 6). (G) Transcription profiles of relevant genes following treatment with DMSO or 5 μ M RSL3 (n = 4). (H) Transcription profiles of relevant genes following treatment with DMSO or 5 μ M OSU-T315 (n = 4). The data were analyzed by two-tailed Student's *t*-test (A,B), one-way ANOVA corrected by Dunnett's (G,H) test, and two-way ANOVA corrected by Tukey's (C,F) and Sidak's (D,E) test. Complex pairwise comparison results are presented using the Compact Letter Display (CLD) in (C) and (F). ns, not significant; * *p* < 0.05, ** *p* < 0.01, *** *p* < 0.001, **** *p* < 0.0001.

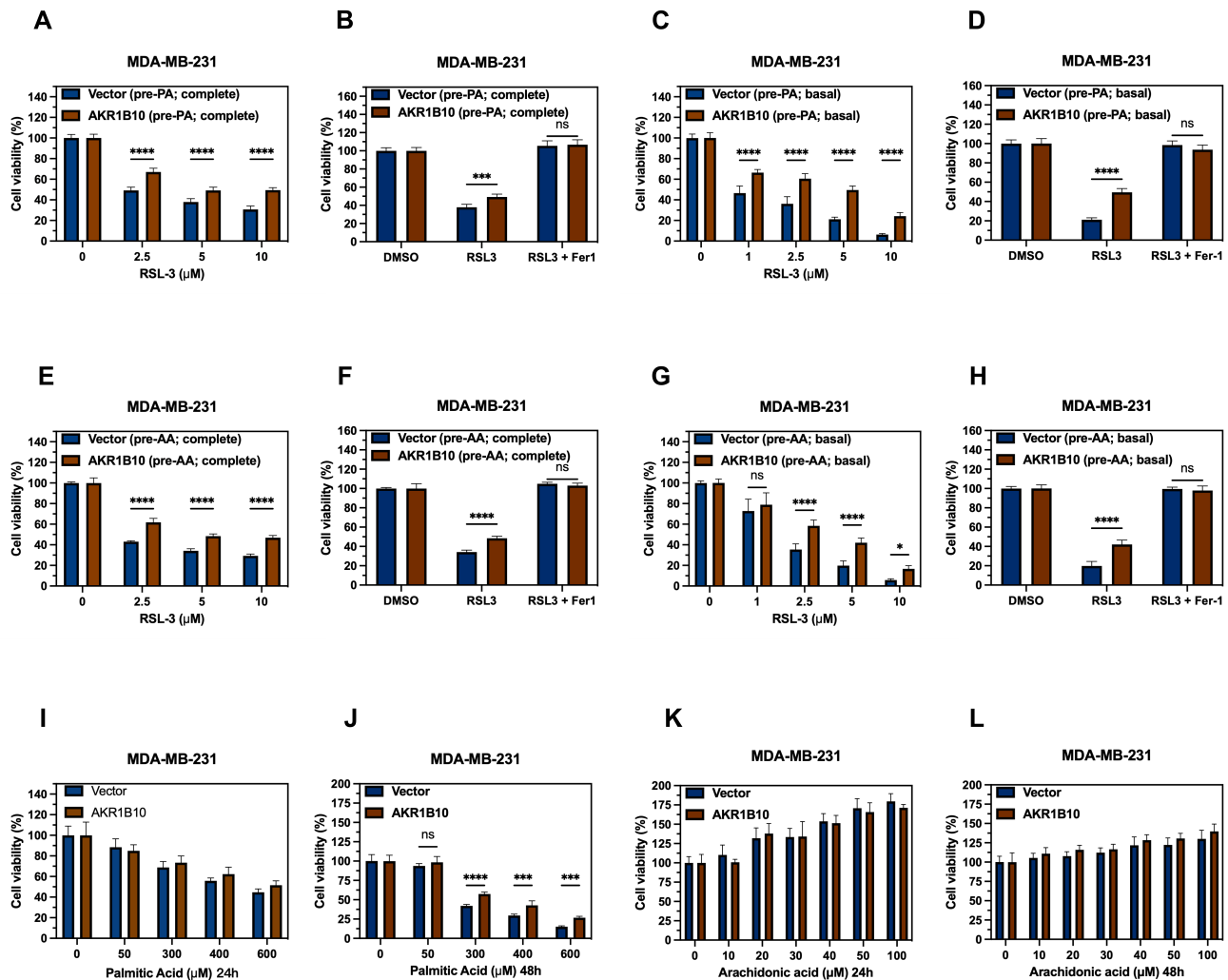


Fig. 4. AKR1B10 influences the efficacy of RSL3 therapy in the presence of different exogenous fatty acids. (A) MDA-MB-231 cells with or without overexpression of AKR1B10 were pre-incubated with 300 μ M palmitic acid (PA) in complete culture medium for 2 h, followed by treatment with varying concentrations of RSL3 for 24 h. (B) MDA-MB-231 cells with or without high expression of AKR1B10 were pre-incubated with 300 μ M PA in complete culture medium for 2 h, followed by 5 μ M RSL3 for 24 h. Fer-1 was used to rescue from cell death. (C) MDA-MB-231 cells with or without high expression of AKR1B10 were pre-incubated with 300 μ M PA in basal culture medium for 2 h, followed by treatment with varying concentrations of RSL3 in complete medium for 24 h; (D) MDA-MB-231 cells with or without high expression of AKR1B10 were pre-incubated with 300 μ M PA in basal culture medium for 2 h, followed by 5 μ M RSL3 in complete medium for 24 h. Fer-1 was used to rescue from cell death. (E–H) Using a treatment regimen analogous to that employed in (A–D) pre-incubation was carried out with 50 μ M arachidonic acid (AA). Extended culture with varying concentrations of PA (I,J). Extended culture with varying concentrations of AA (K,L). In all experiments, the CCK8 assay was utilized to measure cell viability ($n = 6$). The data were analyzed by two-way ANOVA corrected by Sidak's test. ns, not significant; * $p < 0.05$, *** $p < 0.001$, **** $p < 0.0001$.

induced by the combined treatments (Fig. 4A–H). To assess whether the fatty acid concentrations used were cytotoxic, the cells underwent prolonged culture with either PA or AA alone. After 24 h of exposure to PA at concentrations ranging from 0 to 600 μ M, the overexpression of AKR1B10 showed no significant effect on cell viability (Fig. 4I). However, after 48 h of incubation, AKR1B10 conferred protection against lipid toxicity induced by PA at a concentration of 300 μ M ($p < 0.0001$) (Fig. 4J). In contrast, the expres-

sion of AKR1B10 had no significant impact on cell viability after 24 h (Fig. 4K) and 48 h (Fig. 4L) of treatment with AA at concentrations ranging from 0 to 100 μ M. After 24 h of combined treatment, the fatty acid concentrations used here did not result in a significant difference in cell viability between cell lines with or without AKR1B10 overexpression. These findings indicate that both PA and AA fatty acids can sensitize cells to ferroptosis and that AKR1B10 is a protective factor against ferroptosis.

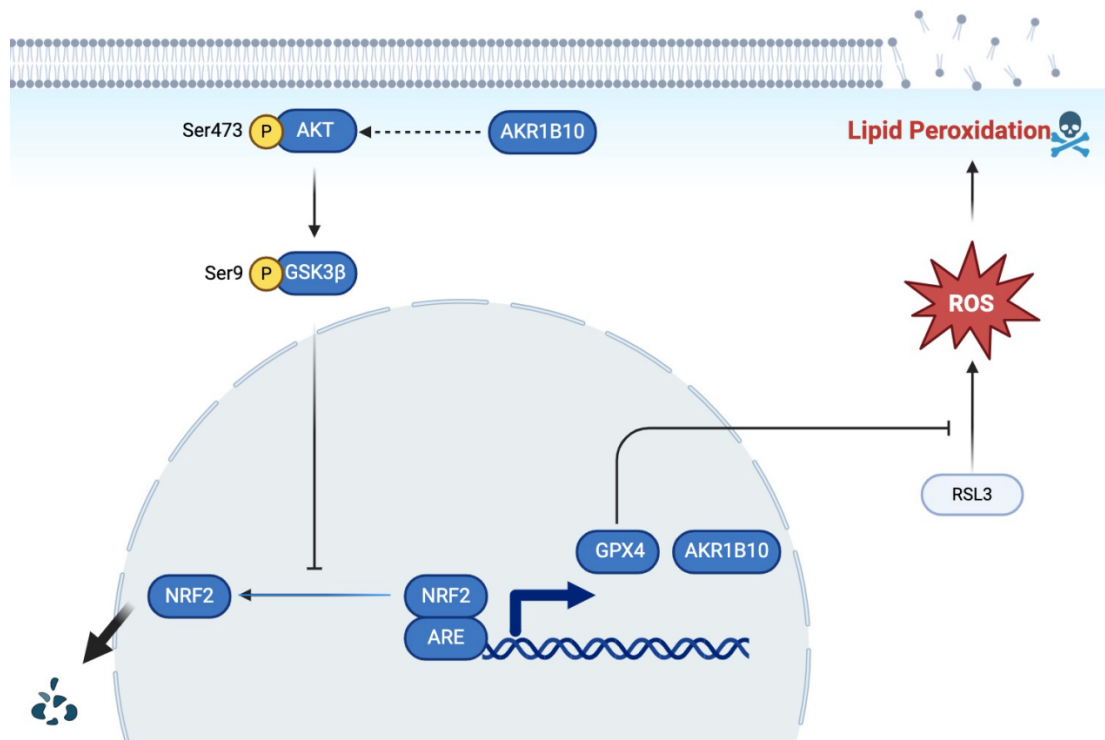


Fig. 5. Ectopic expression of AKR1B10 enables cells to survive in ferroptosis. This figure was created using the website www.biorender.com.

3.5 Proposed Mechanism by Which Ectopic Expression of AKR1B10 Favors Cell Survival During Ferroptosis

In summary, our results suggest that AKR1B10 can activate the NRF2-mediated antioxidant pathway via phosphorylation of the AKT/GSK3 β pathway, thereby increasing the GPX4 protein level and protecting triple-negative breast cancer MDA-MB-231 cells from ferroptosis (Fig. 5).

4. Discussion

This study demonstrated that AKR1B10 regulates ferroptosis in MDA-MB-231 cells via the AKT/GSK3 β /NRF2/GPX4 axis. The expression level of GPX4 protein is regulated by various factors, with numerous enzymes and proteins interacting within the ferroptosis pathway. Key components of this pathway are regulated by the transcription factor NRF2, including GPX4, the cystine/glutamate transporter xc- (SLC7A11), HO-1, glutamate-cysteine ligase (GCLC), ferritin, transferrin receptor 1 (TfR1), and ferroporter (Fpn) [17]. Additionally, the stability of GPX4 is regulated by mechanisms including degradation by ubiquitination, as well as autophagic degradation. In eukaryotes, the ubiquitin-proteasome system (UPS) and selective degradation by the autophagy system maintain the homeostasis of cellular macromolecular proteins. However, the cellular response to ferroptosis can depend on the specific cargos degraded by this system. The UPS degrades key ferroptosis inhibitors such as SLC7A11 and GPX4, while selective autophagy targets cargos like ferritin, GPX4, circadian proteins, and lipid droplets [18].

GPX4 degradation via ubiquitination has been shown to increase the sensitivity of TNBC cells to ferroptosis [19].

In the resting state, the UPS continuously degrades NRF2. Its interaction with KEAP1 facilitates this process by linking NRF2 to the ubiquitin ligase complex. However, exposure to stressors such as ROS modifies KEAP1 cysteine residues, resulting in functional inactivation. This modification stabilizes NRF2, enabling its nuclear translocation and subsequent activation of protective gene transcription. Under conditions of p62 overproduction or impaired autophagy, binding of p62 to the KEAP1-NRF2 interaction site stabilizes NRF2 and promotes the transcription of its target genes [20]. Significant accumulation of NRF2 was observed in the nucleus of ATG7-deficient (autophagy-deficient) hepatocytes. In pancreatic ductal adenocarcinoma (PDA) with a high incidence of activating *KRAS* mutations and *TP53* inactivation, NRF2 controls cellular fate by inducing the expression of antioxidant genes expression under conditions of oxidative stress [21].

In a mouse model of breast cancer metastasis, HK2 was found to bind to the protein kinase GSK3 β , effectively isolating it from other cellular components. This segregation facilitates the phosphorylation of GSK3 β , which in turn affects the expression levels of various proteins that it regulates, including NRF2, SNAIL, and MCL1 [22]. NRF2 in turn regulates detoxification enzymes, drug transporters, anti-apoptotic factors, and proteasomes. These proteins are essential for the cellular response to stress and injury, thus helping to maintain normal cell functions. Nrf2 contains

phosphorylation consensus motifs for GSK3 β , making it a potential substrate for this kinase [23]. Novel therapeutic approaches in breast cancer could involve the modulation of GSK3 β phosphorylation or direct targeting of the regulatory mechanism of NRF2. Our findings showed that the AKR1B10 protein expression level during resting phases varied relative to the AKT/GSK3 β /NRF2/GPX4 axis, as well as during ferroptosis triggered by RSL3. This suggests potential applications for AKR1B10 in the diagnosis and treatment of tumors where its expression is elevated.

The serine-threonine kinase GSK3 plays a central role in a variety of cellular processes. TNBC is a more aggressive subtype of breast cancer that exhibits gene expression profiles similar to those found in cells that have undergone epithelial-mesenchymal transition (EMT). GSK3 β inhibitors can suppress cells with mesenchymal and stem cell phenotypes. Moreover, EMT and tumor stem cell characteristics are fundamental to treatment resistance and tumor recurrence [24]. OSU-T315 is a novel targeted drug that promotes the dephosphorylation of AKT Ser473 and GSK3 β Ser9. It also directly inhibits the membrane translocation and activation of AKT through a unique molecular mechanism of action [25]. The present study is the first to report that OSU-T315 differentially regulates GPX4 and other NRF2-related detoxification proteins through the AKT/GSK3 β /NRF2 signaling pathway. This was observed in MDA-MB-231 tumor cells with high AKR1B10 expression, as well as those with low expression.

Significant therapeutic effects may be obtained by combining exogenous fatty acids with the process of ferroptosis. Exogenous fatty acids can modulate lipid metabolism in cells, alter membrane fluidity, and enhance their sensitivity to ferroptosis, thus improving the anti-cancer efficacy. Highly saturated membrane lipids help to protect cancer cells from the harmful effects of ROS. This is because saturated lipids are less likely to undergo oxidation compared to unsaturated lipids, making them more stable and better able to prevent damage. PUFAs are highly susceptible to oxidation during ferroptosis, especially AA and adrenic acid. Oxidation leads to disruption of the lipid bilayer, thereby compromising cell membrane function. Lipid peroxidation of PUFAs is a key factor in promoting cell lysis and death, and interactions among multiple complex lipid metabolism pathways strongly impact the vulnerability of cells to ferroptosis [26].

MDA-MB-231 cells are a widely studied cell line derived from TNBC. They appear to have greater sensitivity to the lipid microenvironment than MCF7 cells, which are a Luminal type A breast cancer cell line. PA and docosahexaenoic acid (DHA) can remodel the endoplasmic reticulum (ER) membrane of MDA-MB-231 cells, thereby affecting the activity of certain resident enzymes. This difference in sensitivity to the lipid environment may account for variations in chemoresistance between breast cancer cell lines [27].

The PI3K/AKT/mTOR signaling pathway is crucial for the regulation of a wide range of cellular functions, including lipid metabolism. A study on the effects of various free fatty acids (FFAs) found that PA could reduce basal PI3K activity in MDA-MB-231 cells [28]. Furthermore, increased activity of nicotinamide adenine dinucleotide phosphate (NADPH) oxidase, leading to the generation of ROS and triggering of ferroptosis, was observed in both *in vitro* and *in vivo* models of myocardial lipotoxicity following exposure to PA and to a long-term high-fat diet (HFD) [29]. Targeting of the AKT/GSK3 β signaling pathway to increase phosphorylation resulted in decreased lipid peroxidation and mitochondrial ROS levels, thereby attenuating PA-induced cardiomyocyte ferroptosis [30].

AA shows varied therapeutic effects in different tumor types, including a dose-dependent effect on multiple myeloma (MM) cells. Compared to vehicle controls, high doses of AA significantly reduced the proliferation and viability of MM cells, whereas low doses had the opposite effect. The active metabolites of AA support cellular function, but AA also serves as a precursor for the generation of oxygen radicals that damage cells via peroxidation. A 50 μ M dose of AA was shown to increase lipid peroxidation in MM cells [31]. Interferon gamma (IFN- γ) produced by T cells can bind to AA in tumor cells and induce immunogenic ferroptosis [32]. Low doses of AA can amplify these ferroptosis effects and improve anti-tumor immune responses, regardless of whether they are spontaneous or induced by immune checkpoint blockade (ICB).

Wang *et al.* [33] reported that knockdown of AKR1B10 in tumor cells resulted in a reduction of more than 50% in total cellular lipids, especially phospholipids, along with an increase in intracellular lipid peroxides. It was further revealed that AKR1B10 helps to maintain acetyl-CoA carboxylase α (ACCA), which subsequently affects fatty acid synthesis. The other study has demonstrated that saturated or cis-unsaturated fatty acids inhibit the activity of AKR1B10. In HCT-15 cells, the metabolism of 4-oxo-2-nonenal mediated by AKR1B10 is effectively blocked by oleic acid (OA) and AA [34]. The present study found that combining RSL3 with PA or AA can induce tumor cell death, while AKR1B10 serves as a protective factor against ferroptosis.

Despite many advances in diagnosis, surgery, radiotherapy, and chemotherapy, the management of breast cancer, and in particular TNBC remains challenging and patient survival rates are still quite poor. TNBC displays a heterogeneous phenotype, particularly in terms of ferroptosis-related metabolites and metabolic pathways [35]. It is therefore crucial to identify other potential forms of cell death in order to find new biomarkers or therapeutic targets and thus overcome tumor chemoresistance. The research presented here provides better understanding of the role of AKR1B10 in TNBC and offers new perspectives and potential targets for related therapeutic strategies.

5. Conclusion

This study provides new evidence showing that AKR1B10 can protect tumor cells from ferroptosis. The underlying mechanism may be related to the AKT Ser473/GSK3 β Ser9/NRF2/GPX4 pathway. AKR1B10 appears to be a crucial determinant for the therapeutic efficacy of RSL3 under different exogenous fatty acid microenvironments.

Availability of Data and Materials

The researchers affirm that all information underpinning the findings of this investigation are accessible. The source data can be obtained from the corresponding authors upon reasonable request.

Author Contributions

SWU, QL and DL conceived and designed the experiments. SWU, GY, YL, SWANG and JW performed the experiments. SWU, GY, XW, QL and DL analyzed the data. SWU, QL and DL drafted and revised the manuscript. All authors approved the final version of the manuscript. All authors contributed to editorial changes in the manuscript. All authors have participated sufficiently in the work and agreed to be accountable for all aspects of the work.

Ethics Approval and Consent to Participate

Not applicable.

Acknowledgment

The authors express their gratitude to the Medical Research Centre of Shenzhen Nanshan People's Hospital for granting access to the experimental facilities. We also extend our thanks to Dr. Wen Ai and Mr. Yongshen He for their invaluable support.

Funding

This research received financial support from the following funding sources: General Projects of the National Natural Science Foundation of China (82273236), Guangdong Basic and Applied Basic Research Foundation (2022A1515220042), the Basic and Applied Basic Research Foundation of Guangdong Province (2023A1515030182), Shenzhen Natural Science Foundation Project (JCYJ20220530141609021), Supported by Municipal Financia 1 Subsidy of Shenzhen Medical Key Discipline Construction (SZXK054) and the Project of Technological Research and Development and Creative Design Itemized Fund (NS2024030).

Conflict of Interest

The authors declare no conflict of interest.

Supplementary Material

Supplementary material associated with this article can be found, in the online version, at <https://doi.org/10.31083/FBL36615>.

References

- [1] Dixon SJ, Lemberg KM, Lamprecht MR, Skouta R, Zaitsev EM, Gleason CE, *et al.* Ferroptosis: an iron-dependent form of nonapoptotic cell death. *Cell*. 2012; 149: 1060–1072. <https://doi.org/10.1016/j.cell.2012.03.042>.
- [2] Yunchu Y, Miyanaga A, Seike M. Integrative Analysis of Ferroptosis-Related Genes in Small Cell Lung Cancer for the Identification of Biomarkers and Therapeutic Targets. *Frontiers in Bioscience (Landmark edition)*. 2023; 28: 125. <https://doi.org/10.31083/j.fbl2806125>.
- [3] Huang M, Wang Y, Wu X, Li W. Crosstalk between Endoplasmic Reticulum Stress and Ferroptosis in Liver Diseases. *rontiers in Bioscience (Landmark edition)*. 2024; 29: 221. <https://doi.org/10.31083/j.fbl2906221>.
- [4] Chen X, Li J, Kang R, Klionsky DJ, Tang D. Ferroptosis: machinery and regulation. *Autophagy*. 2021; 17: 2054–2081. <https://doi.org/10.1080/15548627.2020.1810918>.
- [5] Yang WS, SriRamaratnam R, Welsch ME, Shimada K, Skouta R, Viswanathan VS, *et al.* Regulation of ferroptotic cancer cell death by GPX4. *Cell*. 2014; 156: 317–331. <https://doi.org/10.1016/j.cell.2013.12.010>.
- [6] Maiorino M, Conrad M, Ursini F. GPx4, Lipid Peroxidation, and Cell Death: Discoveries, Rediscoveries, and Open Issues. *Antioxidants & Redox Signaling*. 2018; 29: 61–74. <https://doi.org/10.1089/ars.2017.7115>.
- [7] Stamenkovic A, O'Hara KA, Nelson DC, Maddaford TG, Edel AL, Maddaford G, *et al.* Oxidized phosphatidylcholines trigger ferroptosis in cardiomyocytes during ischemia-reperfusion injury. *American Journal of Physiology. Heart and Circulatory Physiology*. 2021; 320: H1170–H1184. <https://doi.org/10.1152/ajpheart.00237.2020>.
- [8] Spite M, Baba SP, Ahmed Y, Barski OA, Nijhawan K, Pettrash JM, *et al.* Substrate specificity and catalytic efficiency of aldo-keto reductases with phospholipid aldehydes. *The Biochemical Journal*. 2007; 405: 95–105. <https://doi.org/10.1042/BJ20061743>.
- [9] Huang C, Verhulst S, Shen Y, Bu Y, Cao Y, He Y, *et al.* AKR1B10 promotes breast cancer metastasis through integrin $\alpha 5/\delta$ -catenin mediated FAK/Src/Rac1 signaling pathway. *Oncotarget*. 2016; 7: 43779–43791. <https://doi.org/10.18632/oncotarget.9672>.
- [10] Cao Z, Delfino K, Tiwari V, Wang X, Hannan A, Zaidi F, *et al.* AKR1B10 as a Potential Novel Serum Biomarker for Breast Cancer: A Pilot Study. *Frontiers in Oncology*. 2022; 12: 727505. <https://doi.org/10.3389/fonc.2022.727505>.
- [11] Furukawa M, Xiong Y. BTB protein Keap1 targets antioxidant transcription factor Nrf2 for ubiquitination by the Cullin 3-Roc1 ligase. *Molecular and Cellular Biology*. 2005; 25: 162–171. <https://doi.org/10.1128/MCB.25.1.162-171.2005>.
- [12] Liao S, Wu J, Liu R, Wang S, Luo J, Yang Y, *et al.* A novel compound DBZ ameliorates neuroinflammation in LPS-stimulated microglia and ischemic stroke rats: Role of Akt(Ser473)/GSK3 β (Ser9)-mediated Nrf2 activation. *Redox Biology*. 2020; 36: 101644. <https://doi.org/10.1016/j.redox.2020.101644>.
- [13] Penning TM. Aldo-Keto Reductase Regulation by the Nrf2 System: Implications for Stress Response, Chemotherapy Drug Resistance, and Carcinogenesis. *Chemical Research in Toxicology*. 2017; 30: 162–176. <https://doi.org/10.1021/acs.chemrestox.6b00319>.
- [14] Lee SL, Hsu EC, Chou CC, Chuang HC, Bai LY, Kulp SK, *et al.*

- Identification and characterization of a novel integrin-linked kinase inhibitor. *Journal of Medicinal Chemistry*. 2011; 54: 6364–6374. <https://doi.org/10.1021/jm2007744>.
- [15] van Weverwijk A, Koundouros N, Irvani M, Ashenden M, Gao Q, Poulgiannis G, *et al.* Metabolic adaptability in metastatic breast cancer by AKR1B10-dependent balancing of glycolysis and fatty acid oxidation. *Nature Communications*. 2019; 10: 2698. <https://doi.org/10.1038/s41467-019-10592-4>.
- [16] Pascual G, Avgustinova A, Mejetta S, Martín M, Castellanos A, Attolini CSO, *et al.* Targeting metastasis-initiating cells through the fatty acid receptor CD36. *Nature*. 2017; 541: 41–45. <https://doi.org/10.1038/nature20791>.
- [17] Kajarabille N, Latunde-Dada GO. Programmed Cell-Death by Ferroptosis: Antioxidants as Mitigators. *International Journal of Molecular Sciences*. 2019; 20: 4968. <https://doi.org/10.3390/ijms20194968>.
- [18] Chen X, Yu C, Kang R, Kroemer G, Tang D. Cellular degradation systems in ferroptosis. *Cell Death and Differentiation*. 2021; 28: 1135–1148. <https://doi.org/10.1038/s41418-020-00728-1>.
- [19] Ding Y, Chen X, Liu C, Ge W, Wang Q, Hao X, *et al.* Identification of a small molecule as inducer of ferroptosis and apoptosis through ubiquitination of GPX4 in triple negative breast cancer cells. *Journal of Hematology & Oncology*. 2021; 14: 19. <https://doi.org/10.1186/s13045-020-01016-8>.
- [20] Komatsu M, Kurokawa H, Waguri S, Taguchi K, Kobayashi A, Ichimura Y, *et al.* The selective autophagy substrate p62 activates the stress responsive transcription factor Nrf2 through inactivation of Keap1. *Nature Cell Biology*. 2010; 12: 213–223. <https://doi.org/10.1038/ncb2021>.
- [21] Chio IIC, Jafarnejad SM, Ponz-Sarvisé M, Park Y, Rivera K, Palm W, *et al.* NRF2 Promotes Tumor Maintenance by Modulating mRNA Translation in Pancreatic Cancer. *Cell*. 2016; 166: 963–976. <https://doi.org/10.1016/j.cell.2016.06.056>.
- [22] Blaha CS, Ramakrishnan G, Jeon SM, Nogueira V, Rho H, Kang S, *et al.* A non-catalytic scaffolding activity of hexokinase 2 contributes to EMT and metastasis. *Nature Communications*. 2022; 13: 899. <https://doi.org/10.1038/s41467-022-28440-3>.
- [23] Jiang Y, Bao H, Ge Y, Tang W, Cheng D, Luo K, *et al.* Therapeutic targeting of GSK3 β enhances the Nrf2 antioxidant response and confers hepatic cytoprotection in hepatitis C. *Gut*. 2015; 64: 168–179. <https://doi.org/10.1136/gutjnl-2013-306043>.
- [24] Vijay GV, Zhao N, Den Hollander P, Toneff MJ, Joseph R, Pietila M, *et al.* GSK3 β regulates epithelial-mesenchymal transition and cancer stem cell properties in triple-negative breast cancer. *Breast Cancer Research: BCR*. 2019; 21: 37. <https://doi.org/10.1186/s13058-019-1125-0>.
- [25] Liu TM, Ling Y, Woyach JA, Beckwith K, Yeh YY, Hertlein E, *et al.* OSU-T315: a novel targeted therapeutic that antagonizes AKT membrane localization and activation of chronic lymphocytic leukemia cells. *Blood*. 2015; 125: 284–295. <https://doi.org/10.1182/blood-2014-06-583518>.
- [26] Li D, Li Y. The interaction between ferroptosis and lipid metabolism in cancer. *Signal Transduction and Targeted Therapy*. 2020; 5: 108. <https://doi.org/10.1038/s41392-020-00216-5>.
- [27] Rizzo AM, Colombo I, Montorfano G, Zava S, Corsetto PA. Exogenous Fatty Acids Modulate ER Lipid Composition and Metabolism in Breast Cancer Cells. *Cells*. 2021; 10: 175. <https://doi.org/10.3390/cells10010175>.
- [28] Hardy S, Langelier Y, Prentki M. Oleate activates phosphatidylinositol 3-kinase and promotes proliferation and reduces apoptosis of MDA-MB-231 breast cancer cells, whereas palmitate has opposite effects. *Cancer Research*. 2000; 60: 6353–6358.
- [29] Ni X, Duan L, Bao Y, Li J, Zhang X, Jia D, *et al.* Circ_005077 accelerates myocardial lipotoxicity induced by high-fat diet via CyPA/p47PHOX mediated ferroptosis. *Cardiovascular Diabetology*. 2024; 23: 129. <https://doi.org/10.1186/s12933-024-02204-3>.
- [30] Bian J, Ding Y, Wang S, Jiang Y, Wang M, Wei K, *et al.* Celastrol confers ferroptosis resistance via AKT/GSK3 β signaling in high-fat diet-induced cardiac injury. *Free Radical Biology & Medicine*. 2023; 200: 36–46. <https://doi.org/10.1016/j.freeradbiomed.2023.03.004>.
- [31] Panaroni C, Fulzele K, Mori T, Siu KT, Onyewadume C, Maebius A, *et al.* Multiple myeloma cells induce lipolysis in adipocytes and uptake fatty acids through fatty acid transporter proteins. *Blood*. 2022; 139: 876–888. <https://doi.org/10.1182/blood.2021013832>.
- [32] Liao P, Wang W, Wang W, Kryczek I, Li X, Bian Y, *et al.* CD8 $^{+}$ T cells and fatty acids orchestrate tumor ferroptosis and immunity via ACSL4. *Cancer Cell*. 2022; 40: 365–378.e6. <https://doi.org/10.1016/j.ccell.2022.02.003>.
- [33] Wang C, Yan R, Luo D, Watabe K, Liao DF, Cao D. Aldo-keto reductase family 1 member B10 promotes cell survival by regulating lipid synthesis and eliminating carbonyls. *The Journal of Biological Chemistry*. 2009; 284: 26742–26748. <https://doi.org/10.1074/jbc.M109.022897>.
- [34] Hara A, Endo S, Matsunaga T, Soda M, El-Kabbani O, Yashiro K. Inhibition of aldo-keto reductase family 1 member B10 by unsaturated fatty acids. *Archives of Biochemistry and Biophysics*. 2016; 609: 69–76. <https://doi.org/10.1016/j.abb.2016.09.010>.
- [35] Yang F, Xiao Y, Ding JH, Jin X, Ma D, Li DQ, *et al.* Ferroptosis heterogeneity in triple-negative breast cancer reveals an innovative immunotherapy combination strategy. *Cell Metabolism*. 2023; 35: 84–100.e8. <https://doi.org/10.1016/j.cmet.2022.09.021>.